Astronomy & Astrophysics manuscript no. paper
August 7, 2007

Double-detonation supernovae of sub-Chandrasekhar mass white dwarfs

M. Fink, W. Hillebrandt, and F. K. Röpke

Max-Planck-Institut für Astrophysik, Karl-Schwarzschild-Str. 1, D-85741 Garching, Germany

Received . . . / Accepted . . .

ABSTRACT

Context. Type Ia supernovae are believed to be white dwarfs disrupted by a thermonuclear explosion. Here we investigate the scenario in which a rather low-mass carbon-oxygen (C + O) white dwarf accumulates helium on its surface in an amount sufficient to ignite a detonation in the helium shell before the Chandrasekhar mass is reached. In principle, this can happen on white dwarfs accreting from a non-degenerate companion, or by merging a C + O white dwarf with a low-mass helium one. In this scenario, the helium detonation is thought to trigger a secondary detonation in the C + O core. It is therefore called the "double-detonation sub-Chandrasekhar" supernova model.

Aims. By means of a set of numerical simulations we investigate the robustness of this explosion mechanism for generic 1-$M_\odot$ models and analyze its observable predictions. Also a resolution dependence in numerical simulations is analyzed.

Methods. Hydrodynamic simulations of the double-detonation sub-Chandrasekhar scenario are conducted in two and three spatial dimensions. The propagation of thermonuclear detonation fronts, both in helium and in the carbon-oxygen mixture, is computed by means of a level-set function and a reduced nuclear reaction network. The decision of whether or not a secondary detonation is triggered in the white dwarf's core is made based on criteria given in the literature.

Results. In a parameter study involving different initial flame geometries for He-shell masses of 0.2 and 0.1 $M_\odot$ (and thus 0.8 and 0.9 $M_\odot$ of C + O) we find that a secondary detonation ignition is a very robust process. Converging shock waves originating from the detonation in the He shell generate the conditions sufficient for a detonation near the center of the white dwarf in most of the cases considered. Finally, we follow the complete evolution of three selected models with 0.2 $M_\odot$ of He through the C/O-detonation phase and obtain ^{56}Ni-masses of about 0.40 to 0.45 $M_\odot$.

Conclusions. Although we have not done a complete scan of the possible parameter space, our results show that sub-Chandrasekhar models are no good candidates for normal or sub-luminous type Ia supernovae. The chemical composition of the ejecta features significant amounts of ^{56}Ni in the outer layers at high expansion velocities which is inconsistent with near-maximum spectra.

Key words. supernovae: general – nuclear reactions, nucleosynthesis, abundances – hydrodynamics – methods: numerical

1. Introduction

One of the major uncertainties in modeling type Ia supernovae (SN Ia) originates from the unknown nature of the progenitor systems because neither observations nor theoretical models are yet conclusive (Branch et al. 1995; Ruiz-Lapuente et al. 2000; Livio 2000; Nomoto et al. 2003; Han & Podsiadlowski 2004; Napiwotzki et al. 2005; Stritzinger et al. 2006; Parthasarathy et al. 2007). Over the past years, most studies of thermonuclear supernova explosions focused on models in which a thermonuclear flame is formed by a runaway near the center of a white dwarf (WD), composed of carbon and oxygen, once it has reached the Chandrasekhar mass ($M_{\rm Ch} \sim 1.4\ M_\odot$) by accretion from a non-degenerate companion. Starting out in the sub-sonic deflagration mode of flame propagation, these models were shown to give rise to energetic explosions either in pure turbulence-boosted deflagrations (Reinecke et al. 2002b; Gamezo et al. 2003; Röpke & Hillebrandt 2005; Röpke et al. 2006; Schmidt & Niemeyer 2006; Schmidt et al. 2006; Röpke et al. 2007a) or with a delayed triggering of a supersonic detonation phase (Gamezo et al. 2004; Plewa et al. 2004; Röpke & Niemeyer 2007). There seems to be reasonable agreement of such models with the gross features of observed SNe Ia (Röpke et al. 2007a; Mazzali et al. 2007). However, it remains unclear whether the Chandrasekhar mass model can account for the full range of SN Ia observations. In particular, the mechanism of the sub-luminous events (SN 1991bg being a prototypical example) remains a puzzle (Mazzali et al. 2007). Stritzinger et al. (2006) even claim typical ejecta masses below $M_{\rm Ch}$ for a sample of well observed SNe Ia, with the trend that the low-luminosity explosions eject less mass.

Therefore, a long standing question is whether other progenitor channels contribute to the observed SN Ia sample, and two alternatives have been suggested: the *WD merger* or *double degenerate scenario* (in contrast to single degenerate models, which consist of binaries with only one WD) and the *sub-*

Chandrasekhar model. In the present work we explore the latter.

The basic idea of the sub-Chandrasekhar model is that if the accretion rate onto a WD is lower than about $1 - 4 \cdot 10^{-8}\ M_\odot\ \mathrm{yr}^{-1}$ the accreted He (or the H processed to He) is not fused steadily into C and O. Instead, after reaching a critical amount of He at relatively low densities, the He shell becomes unstable and detonates (cf. Woosley et al. 1986, and references therein). The detonation ignites most likely close to the bottom of the He shell, produces almost pure ^{56}Ni, and can occur long before the WD reaches the Chandrasekhar limit. A second detonation may be triggered spontaneously when the He shell detonation shock wave hits the C + O core or with some delay after the shock has converged near the center of the WD (*double detonation* models). This way, in the sub-Chandrasekhar mass models the conditions for thermonuclear runaway are caused by the compression in the shock wave and not by the high degree of degeneracy as in the Chandrasekhar mass models.

Delayed double detonations have been studied extensively before. Woosley & Weaver (1994), and Livne (1990) carried out one-dimensional (1D) simulations and Livne & Glasner (1990, 1991) considered two-dimensional (2D) setups. In 1D the He detonation ignites synchronously in a layer close to the bottom of the He shell and due to the spherical symmetry constraint the shock converges perfectly in the center. However, this is not a very realistic model. According to Livne (1990) an ignition most likely happens in a single point leading to an off-center convergence of oblique shock waves in the core.

Several other simulations predict successful directly ignited double detonations (Livne 1997; Arnett 1997; Wiggins & Falle 1997; Wiggins et al. 1998). The smoothed particle hydrodynamics simulations by Benz (1997) and García-Senz et al. (1999) were carried out in 3D. They report an increased probability of the direct core ignition if the He detonation does not happen directly at the core–shell interface but at a certain distance above it. This way, the pressure jump can grow large enough before hitting the core.

In this work, the results of a (restricted) parameter study are presented investigating the possibility of triggering the second detonation in two and three dimensions. In all our models the WD has a total mass of 1 $M_\odot$, but the (C + O)-core and the He-shell masses differ. We compute sequences of models with very different initial flame geometries in order to test the robustness of this explosion mechanism. Since this latter question is the main focus of our paper, most of the simulations are stopped once the conditions for a detonation are matched. However, for a few successful cases the energetics and nucleosynthesis of complete double detonations are computed. In the following chapter the model details will be described. Section 3 shows the simulation results, which are summarized and discussed in the last part of the paper.

2. Explosion model

2.1. General setup

The numerical scheme used in our simulations is a modified version of the code described by Reinecke et al. (1999a, 2002a), Röpke & Hillebrandt (2005), Golombek & Niemeyer (2005), and Röpke & Niemeyer (2007). The main difference is the burning physics which accounts for He detonations and the propagation of two detonation waves.

Our hydrodynamic simulations were carried out on a uniform Eulerian grid with a finite volume scheme based on the PROMETHEUS implementation (Fryxell et al. 1989) of the "piecewise parabolic method" (PPM) (Colella & Woodward 1984). Thus, discontinuities like shocks were automatically and accurately captured but, nonetheless, smeared out over several grid cells. A potential concern is the overheating effect observed in Godunov-type schemes when shocks hit walls or collide. Following the suggestion of Donat & Marquina (1996), an approximate Riemann solver (the so-called Marquina solver) was implemented but this did not lead to noticeable differences. Thus, all simulations presented in the following are based on the exact Riemann solver of Colella & Glaz (1985).

While the parameter study testing the possibility of igniting a detonation in the C + O core was carried out on a static grid, the complete double detonation models presented at the end of Sect. 3 employed a co-expanding grid as in Röpke & Hillebrandt (2005) in order to account for the expansion of the WD. The coordinates were (r, z)-cylindrical in 2D and cartesian in 3D.

The equation of state we used includes contributions from an arbitrarily degenerate and arbitrarily relativistic electron gas, a photon gas, electron–positron pairs and nuclei with a Maxwell-Boltzmann distribution. The initial WD was assumed to be in hydrostatic equilibrium. Therefore its structure is uniquely determined once the density at the center and at the core–shell interface and the temperature profile are fixed. For simplicity a constant temperature of $5 \cdot 10^5$ K was assumed throughout the star. Of course, this is an unrealistic choice, but because of the high degree of degeneracy the exact temperature has almost no effect on the state of the matter. Another simplifying assumption is the approximation of the gravitational potential in spherical symmetry. Only the monopole moment of the density distribution averaged over all angles was calculated at every time step.

2.2. Nuclear reactions

In our simulations the detonation flame is approximated as a discontinuity propagating at a certain speed with the fast reactions happening spontaneously at its passage. In this model, only the products of the burning, but not the spatial structure of the detonation, are calculated. As we are mostly interested in the hydrodynamic evolution of the explosion, it is appropriate to use a reduced nuclear network as in Reinecke et al. (2002a). In order to approximate the energy release in the fast reactions and the correct molecular weight of fuel and ashes, it is sufficient to consider only one representative species for each group of elements involved which has a binding energy and mass typical for the group. Our network consists of ^{4}He, a mixture of ^{12}C and ^{16}O with equal mass fractions, ^{28}Si as a representative for the intermediate mass elements, and ^{56}Ni as an iron group element. Nuclear statistical equilibrium in the ashes

was represented by a temperature and density dependent mixture of ^{56}Ni and ^{4}He. The following reactions are included in the model, depending on the density at the front:

- The ^{4}He detonation in the shell produces pure ^{56}Ni. Flame extinction is assumed to occur at $\rho = 10^5$ g cm^{-3}.
- A detonation in the ^{12}C/^{16}O core produces ^{56}Ni in nuclear statistic equilibrium (NSE) with some admixture of ^{4}He at high densities.
- At lower densities the timescale for NSE formation becomes so large that the flame width would be bigger than the extent of the whole core. According to Imshennik & Khokhlov (1984), this is the case at densities of about 10^7 g cm^{-3}. Since it can be assumed that NSE is no longer reached even before the flame width gets close to the extension of the core, $3 \cdot 10^7$ g cm^{-3} instead of 10^7 g cm^{-3} is used as the transition density. At lower density only intermediate-mass elements such as ^{28}Si are produced.
- Below 10^6 g cm^{-3} burning is assumed to cease.

Since the transition density to NSE affects the ^{56}Ni-mass and thus the total explosion energy, its exact value should be investigated further in the future.

In order to distinguish the ^{4}He in the shell from that produced in NSE with ^{56}Ni both are treated as different species in the code. With decreasing densities the ^{4}He in NSE finally recombines to ^{56}Ni. This is the only slow reaction included in our simulations.

The propagation of the detonation flame is modeled with the *"level set technique"* (Osher & Sethian 1988) in the implementation of Golombek & Niemeyer (2005), which in turn is based on the deflagration flame model of Reinecke et al. (1999b). The zero level set of a signed distance function G represents the flame front. Information on whether matter has already been burnt is encoded in its sign. It is negative in the fuel and positive in the ashes. Most important, the location of the flame can be calculated at every time step simply by finding the roots of G. The propagation of the zero level set of G consists of two parts: the advection with the flow and self-propagation by burning, respectively. By means of an operator splitting, the advection of G can be treated in the same way as that of a passive scalar in the hydrodynamic scheme (Mulder et al. 1992; Reinecke et al. 1999a,b). Burning is accounted for by (Reinecke 2001)

$$\left(\frac{\partial G}{\partial t}\right)_{\mathrm{burn}} = s\,|\boldsymbol{\nabla} G|\,.$$

Thus the velocity s of the flame relative to the flux has to be determined at every time step from the quantities on the grid. In the state-of-the-art deflagration codes this is done by an appropriate sub-grid turbulence model. For detonations, as occurring in our models, turbulence effects can be neglected and the propagation speed s can be determined easily as a function of the density ρ only, as will be described in the next section.

The changes in the mass fractions are calculated depending on ρ, when the flame front passes a cell. Here and also in the case of the velocity s we have the problem that in general the state in such a cell is a mixture of a burnt and an unburnt matter. So we have e.g.[1]:

$$\rho = \alpha\rho_1 + (1-\alpha)\rho_2,$$

where α is the volume fraction of the cell occupied by the unburnt state. With the so called *"complete coupling"* scheme the two partial states could be reconstructed from the mixed state (Smiljanovski et al. 1997). This enables flux splitting that avoids numerical mixing of fuel and ashes. While such a scheme has been implemented for 2D small-scale deflagration flame simulations in WD matter (Röpke et al. 2003, 2004a,b), numerical obstacles prevent its application in full star simulations up to now. Here, we apply the "passive implementation" of Reinecke et al. (1999b) and use the mixed state to advect G and also to calculate the burning velocity s and to determine the reaction products.[2]

2.3. Detonation physics

A detonation wave consists of a shock wave that compresses and heats the matter behind it so strongly that it is ignited. The shock wave, in turn, is maintained by the energy released due to burning. Depending on the properties of the reactions taking place, there exist different types of detonations. A very important case is the *Chapman-Jouguet detonation*, which propagates into the fuel at the lowest possible speed. According to Landau & Lifschitz (1991) a detonation that is created spontaneously by the combustion itself is a Chapman-Jouguet detonation in many cases. Therefore, in our simulations we assumed this type of detonation for the He burning. In the Chapman-Jouguet case there exists a simple law for the velocity of the burning front relative to the ashes, which is just equal to the sound speed there:

$$s_{2,\mathrm{He}} = \sqrt{\gamma_2 \left(\frac{\partial p_2}{\partial \rho_2}\right)_T}\,.$$

Here $\gamma = \frac{c_p}{c_V}$ is the ratio of the specific heat at constant pressure and the specific heat at constant volume.

According to Sharpe (1999), self supporting detonations in degenerate carbon/oxygen mixtures at densities between $2 \cdot 10^7$ and $1 \cdot 10^9$ g cm^{-3} are of *pathological* type. These arise in general from a non-monotonic heat release in the reactions. For them the front velocity cannot be determined independent of the reaction rates. Therefore, for the C/O detonations in this work, we used the values calculated by Sharpe (1999) in numerical simulations as a function of density:

$$s_{1,\mathrm{C/O}} = f_{\mathrm{Sharpe}}(\rho).$$

2.4. Ignition conditions in the C + O core

As our code lacks a detailed nuclear network and reaction rates are not calculated, the onset of a C/O detonation can not be

[1] Here and in the following indices 1 and 2 refer to quantities on the unburnt and the burnt side of the front, respectively.

[2] Correctly, one would have to use burning and flow velocities on either the burnt or the unburnt side of the flame to update G due to burning and advection.

Table 1. Critical masses for detonations at given density and temperature according to Niemeyer & Woosley (1997).

ρ [g cm^{-3}]	T_c [10^9 K]	M [g]	R [m]
$2 \cdot 10^9$	2.8	$2.0 \cdot 10^{15}$	0.7
10^8	3.2	$2.0 \cdot 10^{15}$	2
$3 \cdot 10^7$	3.2	$2.0 \cdot 10^{19}$	50

Table 2. Critical temperatures for detonations at given density and mass according to Röpke et al. (2007b). Detonation is impossible for $\rho \leq 1 \cdot 10^6$ g cm^{-3}.

ρ [g cm^{-3}]	T_c [10^9 K]	M [g]	R [km]
10^7	2.8	$2.5 \cdot 10^{23}$	2
10^7	2.0	$2.0 \cdot 10^{25}$	8
10^7	1.9	$1.5 \cdot 10^{27}$	30
$3 \cdot 10^6$	2.3	$2.0 \cdot 10^{28}$	120

followed. Apart from that, in our full star simulations it would not be feasible to resolve the scales of the detonator (where the shock that supports the detonation is built up). Therefore, the decision on whether a detonation is triggered is made upon critical conditions given by Niemeyer & Woosley (1997) and Röpke et al. (2007b) (see Tables 1 and 2). They are based on the following arguments. If there is a sufficiently large region of supersonic spontaneous burning, a strong pressure wave must form and will synchronize with the burning wave if the compression and heating is strong enough to burn the material in the sound crossing time of the region under consideration (Blinnikov & Khokhlov 1986; Woosley 1990; Khokhlov 1991). Therefore a detonation wave is born if that region is big enough or, equivalently, provided that it consists of enough mass at a given density. Niemeyer & Woosley (1997) empirically determined those *critical masses* from hydrodynamic simulations for different densities and for a given linear[3] radial temperature gradient across that mass.[4] Röpke et al. (2007b) used the same code and setup, but determined the critical temperature at a given mass for different densities. They focussed on the low end of possible densities.

3. Simulations

With the numerical scheme described above, several simulations were performed. In Sect. 3.1, the results of a parameter study on the influence of the initial flame geometry for two different core and He-shell masses are presented, followed by a resolution study in Sect. 3.2 and, finally, the determination of explosion energies and nucleosynthesis yields in three successful double detonation simulations. We stress again that the main intension of the parameter study is not to scan the entire parameter space of possible WD properties but rather to investigate the conditions which may lead to a double detonation.

[3] with respect to inner mass

[4] In Table 1 only the results for a mixture of equal mass fractions of C and O are shown. In their work Niemeyer & Woosley (1997) additionally investigated the dependence on the mass fraction.

Table 3. Results of the parameter study about the initial flame geometry. The last column states if the ignition conditions of a core detonation have been reached.

Model	t/s	$T_{9,max}$	$\rho_{8,max}$	Core ignition
s3.60A_2dq_256	0.627	9.09	6.14	yes
s4.10A_2dq_256	0.575	10.2	7.37	yes
s5.00A_2dq_256	0.609	12.1	9.05	yes
r4.24A_2dq_256	0.699	5.62	1.54	yes
r5.00A_2dq_256	0.718	6.00	1.69	yes
z4.24A_2dq_256	0.989	3.27	1.03	no
z5.00A_2dq_256	1.03	3.20	0.981	no
b1A_2dq_256	0.767	4.43	1.32	yes
b2A_2dq_256	0.678	8.61	4.85	yes
b3A_2dq_256	0.674	7.94	4.57	yes
b5iA_2dq_256	0.629	9.53	6.68	yes
b5iiA_2dq_256	0.648	9.00	6.13	yes
b5iiiA_2dq_256	0.648	9.03	6.37	yes
z4.24A_2d_256	1.08	8.53	4.52	yes
s4.30B_2dq_256	0.791	6.82	4.69	yes
s4.80B_2dq_256	0.745	8.17	5.99	yes
r4.50B_2dq_256	0.892	3.96	1.15	no
r5.00B_2dq_256	0.885	4.49	1.23	yes
z4.50B_2dq_256	1.21	2.42	0.808	no
z5.00B_2dq_256	1.24	2.39	0.768	no
b2B_2dq_256	0.855	6.72	4.34	yes
b5iB_2dq_256	0.806	7.63	5.47	yes
z4.50B_2d_256	1.31	6.50	3.38	yes

3.1. Initial flame geometry

The accretion of matter from the companion star onto the WD is a very complex process, and the formation and ignition of a He shell is still afflicted with large uncertainties. As many different initial flame geometries in the shell seem possible, their influence on the possibility and the properties of a double detonation is explored first.

The different initial flame models, which were treated in this study, are shown in Fig. 1 and the nomenclature of the simulations is as follows: The first letter in each model's name denotes the geometry, and the following number specifies it further. "s4.10" means an ignition in a whole layer of the He shell at a radius of 4100 km. "bn" stands for an ignition in n separate "bubbles" (which are, of course, tori in 2D if located off the z-axis). Two special cases of the latter type, for $n = 1$, are "z5.00" and "r5.00", where the initial "bubble" is located at the z- or the r-axis, respectively, at a distance of 5000 km from the origin. Finally the capital letters "A" or "B", which follow the above names, indicate the initial masses which were used:

- Model A: $M_{C/O} = 0.8\ M_\odot$, $M_{He} = 0.2\ M_\odot$,
- Model B: $M_{C/O} = 0.9\ M_\odot$, $M_{He} = 0.1\ M_\odot$.

The results of the study are given in Table 3. There the dimensionality and the number of grid cells along the side of one quadrant are added to the model names. Throughout the study a resolution of 256 cells was used. "2dq" means that only the first quadrant has been simulated assuming equatorial symmetry, whereas "2d" denotes full two dimensional simulations of the whole z-range, capturing the entire WD star.

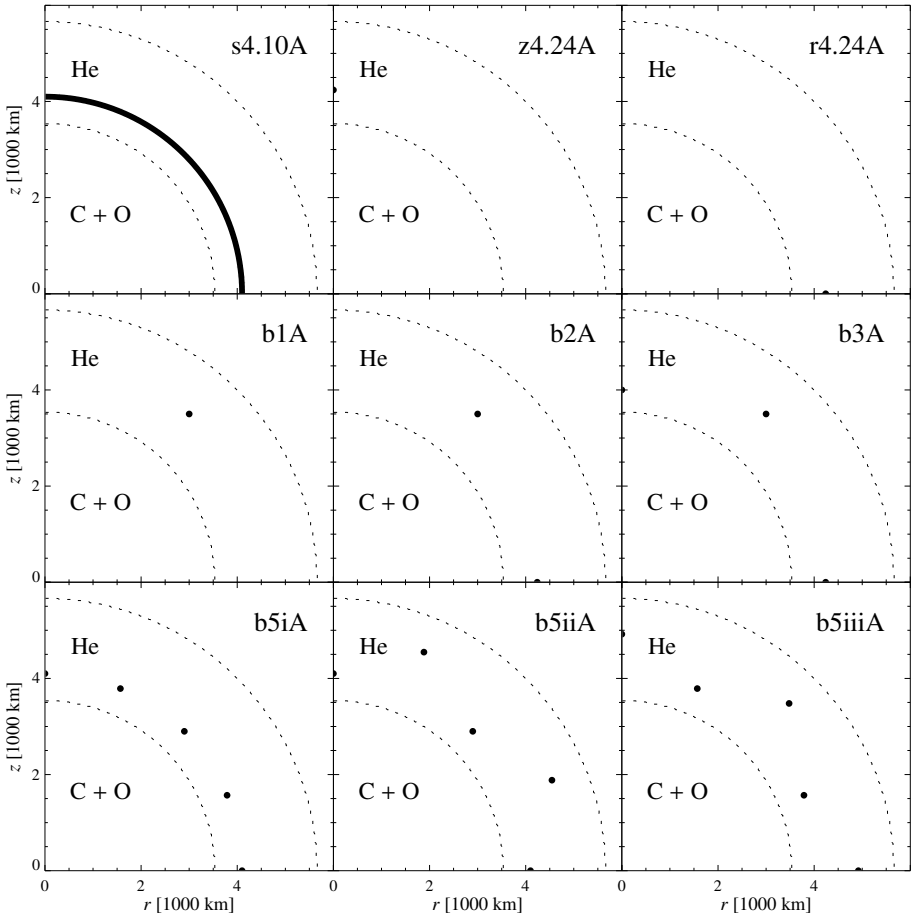

Fig. 1. Initial flame models. The He detonation flame fronts start at the borders of the black regions that already contain hot ashes at the beginning.

The most symmetric case with the simplest hydrodynamic flow pattern is the ignition in a whole layer of the He shell. In model s4.10A_2dq_256 starting with the initial flame geometry shown at the top left of Fig. 1, the inner and the outer spherical detonation front start to propagate inwards and outwards, respectively. While the combustion stops close to the border of the WD due to the low densities, it ceases at the core–shell interface because of the depletion of the He fuel. To investigate the chances of a core ignition, only the hydrodynamic evolution was considered afterwards and all the reactions taking place were stopped. The shock wave that was formerly driving the inner detonation front continues to propagate inwards until it converges at the center. There (at $t = 0.575$ s) a strong shock collision takes place that causes a maximum temperature of $10.2 \cdot 10^9$ K and densities up to $7.37 \cdot 10^8$ g cm^{-3}.

According to Table 1 these maximum values suffice for a C/O ignition, if there is at least a mass of about $2.0 \cdot 10^{15}$ g with the same temperature and density or, more accurately, with a sufficiently small temperature decrease from the above mentioned value. A mass of $2.0 \cdot 10^{15}$ g at this density corresponds to a spherical volume with a radius of the order of 1 km. This length was not resolved in this simulation, where one cell has a diameter of 23.2 km. But as the high temperatures and densities in our simulations are not confined to one single cell, but distributed over several (which means that the region of interest is resolved), the ignition conditions seem to be clearly fulfilled. Consequently, a C/O detonation will occur at the center of the core. There is, however, the possibility that a detonation of the C/O material is triggered already when the shock wave enters at the edge of the core. About 0.1 s after the start of the simulation, temperatures of about 1 to $2 \cdot 10^9$ K and densities of about 10^7 g cm^{-3} are reached. According to Table 2, this is within the range of conditions where a detonation might occur. But as the temperature gradient might possibly be too large across a radius of about 30 km, this question remains open here. A 3D model that successfully ignited directly at the core–shell interface was presented by García-Senz et al. (1999). They observe that this scenario is more likely if the He detonation is not ignited directly at the border to the core but at a certain distance leaving enough time for the pressure jump to grow sufficiently large before reaching the C/O mixture. One-dimensional calculations of Livne & Glasner (1990) came already to the same result.

Our simulations confirm the earlier results. Helium shell detonations were ignited at smaller (s3.60A_2dq_256) and larger (s5.00A_2dq_256) radii than in the case described above. As was expected, the shock wave propagating through the core is weaker in the case of smaller ignition radii and stronger in the case of shocks starting further out. Accordingly the maximum temperatures and densities that are reached in the center are lower in the former and higher in the latter case (see Table 3).

Due to the high degree of symmetry, the models with shell ignition are the ones that can trigger a second detonation most easily. To test multi-dimensional configurations, the complete

ignition layer was replaced by single spots (which effectively are tori in 2D) distributed over the He shell. As far as their maximum densities and temperatures are concerned, the models with five initially ignited bubbles in the first quadrant differ only slightly from the complete shell ignition model (see Table 3). The values of $T_{\max}$ and $\rho_{\max}$ are only slightly lower than for the ignition of a shell, starting at the same radius, and they still match the conditions for a detonation. If the number of initially burning bubbles is reduced to three, peak temperature and density decrease further.

The evolution of simulation b3A_2dq_256 is shown in Fig. 2. Due to the coalescence of the parts of the detonation fronts moving inwards, an almost spherically symmetric shock front is entering the core. This resemblance of the dominant hydrodynamic processes is the reason for the similarity of the results given in Table 3.

In between the bubbles interactions of the detonation shocks take place. The collision process of two radial shocks can be described as a reflection at the plane of symmetry between the waves (see e.g. Courant & Friedrichs 1948). Generally, in this frame the incidence angle may differ from the angle of reflection. This can be seen best at $t = 0.15$ s in Fig. 2. The reflected waves are again reflected at the waves coming from the opposite side of the initial bubble. The repetition of this process should also have some influence on the geometry of the innermost shock front and thus on the conditions given in Table 3.

This can be seen in model b2A_2dq_256, which is similar to model b3A_2dq_256, but with the bubble on the z-axis removed. It starts with only two initially ignited bubbles but reaches greater maximum densities and temperatures in the core. The reason may be a focusing effect on the z-axis in 2D cylindrical symmetry and the bigger density and pressure jump that can build up until the burning reaches the axis.

An analogous focusing effect in the plane of equatorial symmetry (the xy-plane) is not observed. On the contrary, removing the initial burning bubble from the r-axis (i.e. going from b2A_2dq_256 to b1A_2dq_256) leads to a strong decrease of the maximum values of density and temperature.

Considering models with only a single initially burning bubble, the exact geometry of the appearing shock waves is of great importance. After the He detonation has reached the border of the core, it spreads around it in a wave propagating almost perpendicular to the core–shell interface. The detailed hydrodynamic structure has been analyzed in Livne & Glasner (1990), from which Fig. 3 is taken. An oblique shock wave that propagates into the core (tilted by an angle δ with respect to the interface) is associated with the detonation wave moving along the surface of the core. After the shock passage the core–shell interface is also tilted inwards by an angle β. Thus inflowing matter follows the oblique shock. The detonation wave is followed by a rarefaction wave. The angles β and δ can be determined by applying the Rankine-Hugoniot conditions and depend on the strength of the detonation shock.

This structure can clearly be seen at $t = 0.40$ s in model r4.24A_2dq_256, which is the detonation of a torus in the $z = 0$ plane (see Fig. 4). Starting from the "equatorial" plane the detonation wave propagates around the core until it reaches the

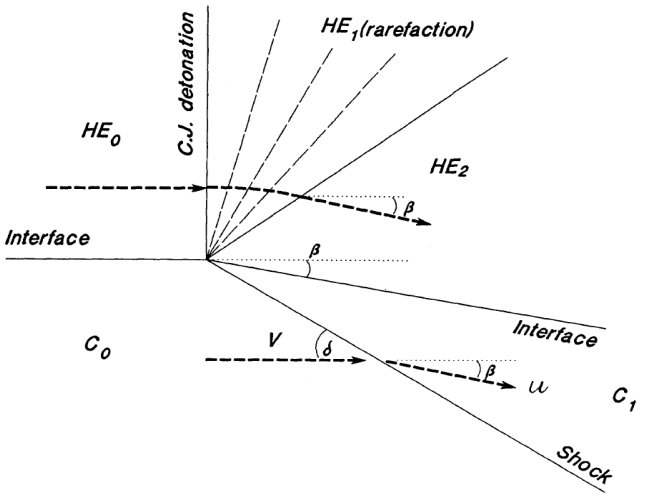

Fig. 3. Structure of a detonation propagating at the core–shell interface in the rest frame of the detonation front from Livne & Glasner (1990). (Here the core consists of carbon only, not of C/O like in our case.)

"polar" z-axis. There a collision of the waves coming from all azimuthal directions takes place. Equivalently, each wave is reflected at the wave coming from the opposite side of the star. This causes the shock wave visible in the last two snapshots of Fig. 4 to propagate to the lower right. In the following the oval inner shock front moves towards the center. At $t = 0.70$ s, even before the center is reached, the maximum density and temperature values are attained on the z-axis at about 850 km away from the center (fourth plot in Fig. 4). The density and temperature values of $1.54 \cdot 10^8$ g cm^{-3} and $5.62 \cdot 10^9$ K are significantly lower than those in the spherically symmetric models, but according to Table 1 they still suffice for the ignition of an off-center core detonation.

In the following simulations, the symmetry of the first detonation was further reduced by departing from equatorial symmetry and simulating a whole rotationally symmetric star, i.e. now the negative z-range was considered too. Fig. 5 shows the example simulation z4.24A_2d_256. Here the He detonation starts in a point on the z-axis and then spreads around the whole WD until it reaches the negative z-axis (see Fig. 5). In this sense, the setup is maximally asymmetric. The processes now taking place are analogous to the simulation r4.24A_2dq_256 described above. But here the maximum density and temperature are reached when the oval inner shock front converges almost perfectly in a "point" on the negative z-axis at $z \approx -1500$ km. Thus at a time of 1.08 s, $\rho_{\max} = 4.52 \cdot 10^8$ g cm^{-3} and $T_{\max} = 8.53 \cdot 10^9$ K are reached. These maximum values are comparable with the spherically symmetric case discussed at the beginning of this section. The reason for this is the high degree of symmetry of the colliding shock fronts. Astoundingly those maximum values are reached comparatively far away from the center in a region of relatively low initial density.

The initial condition considered in the last paragraph seems more realistic than the more symmetric cases. Thus, this model was studied also in simulations with higher numerical resolution. Here, a resolution dependence of the peak temperatures

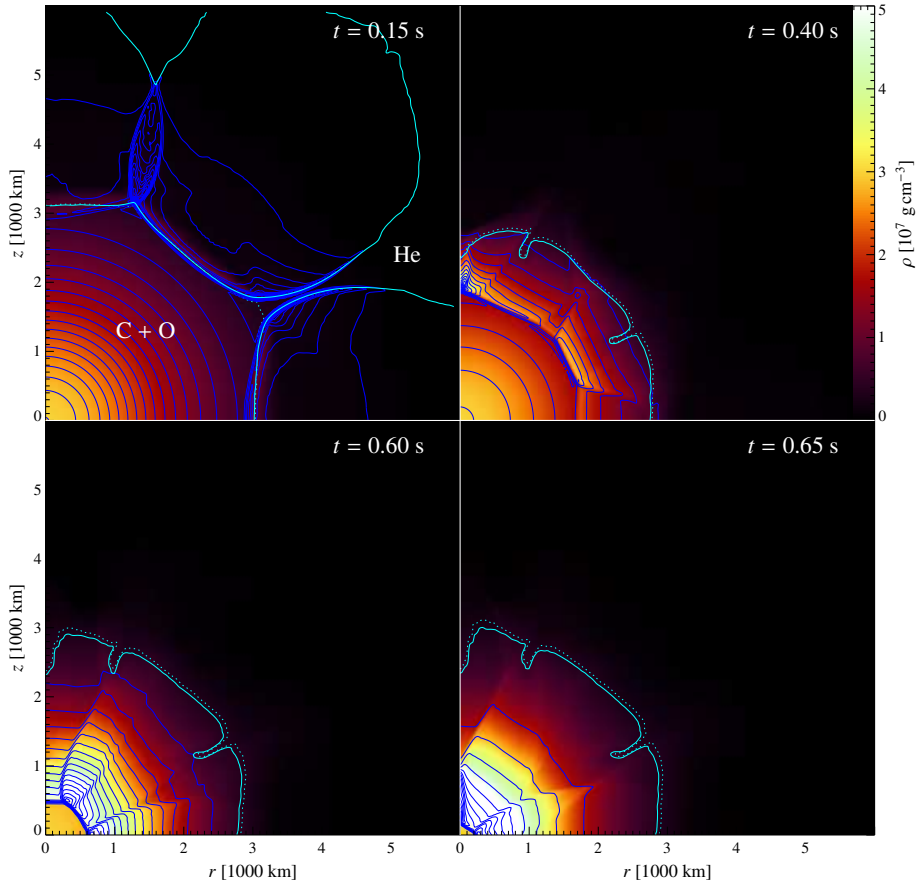

Fig. 2. Time evolution of the model b3A_2dq_256. Here and in the following figures the density is color coded and lines of constant pressure are drawn in blue. In cyan the solid line is the location of the He detonation flame (the zero level of G) and the dashed lines are at the border of the He shell.

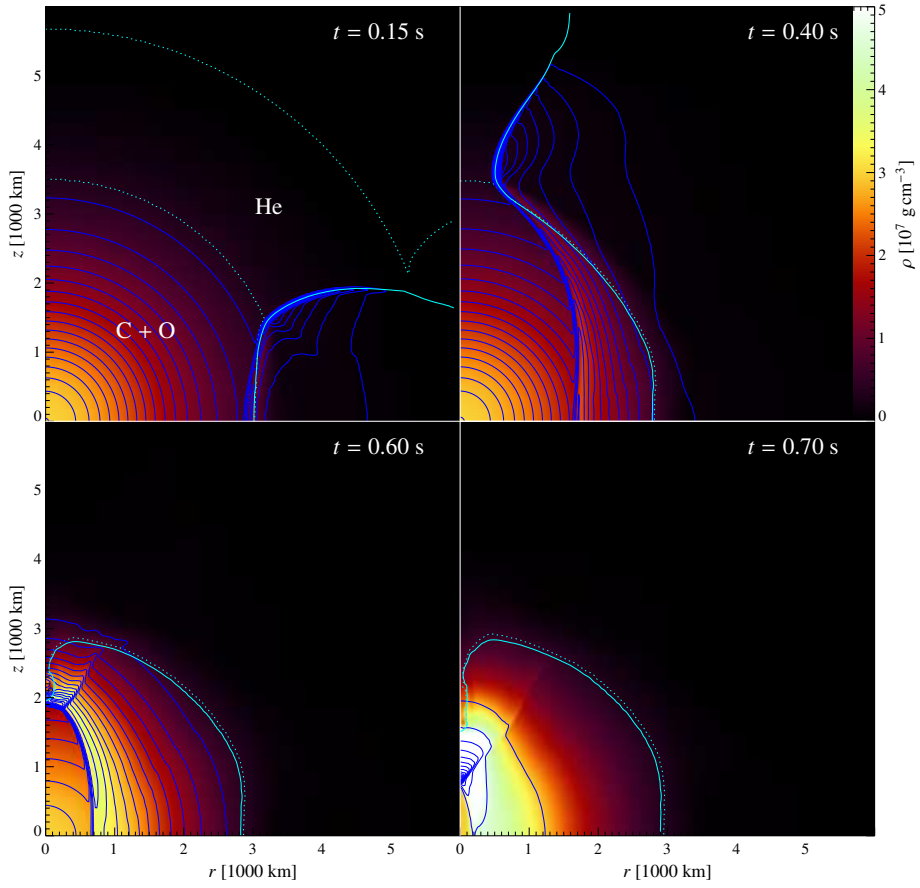

Fig. 4. Time evolution of the model r4.24A_2dq_256.

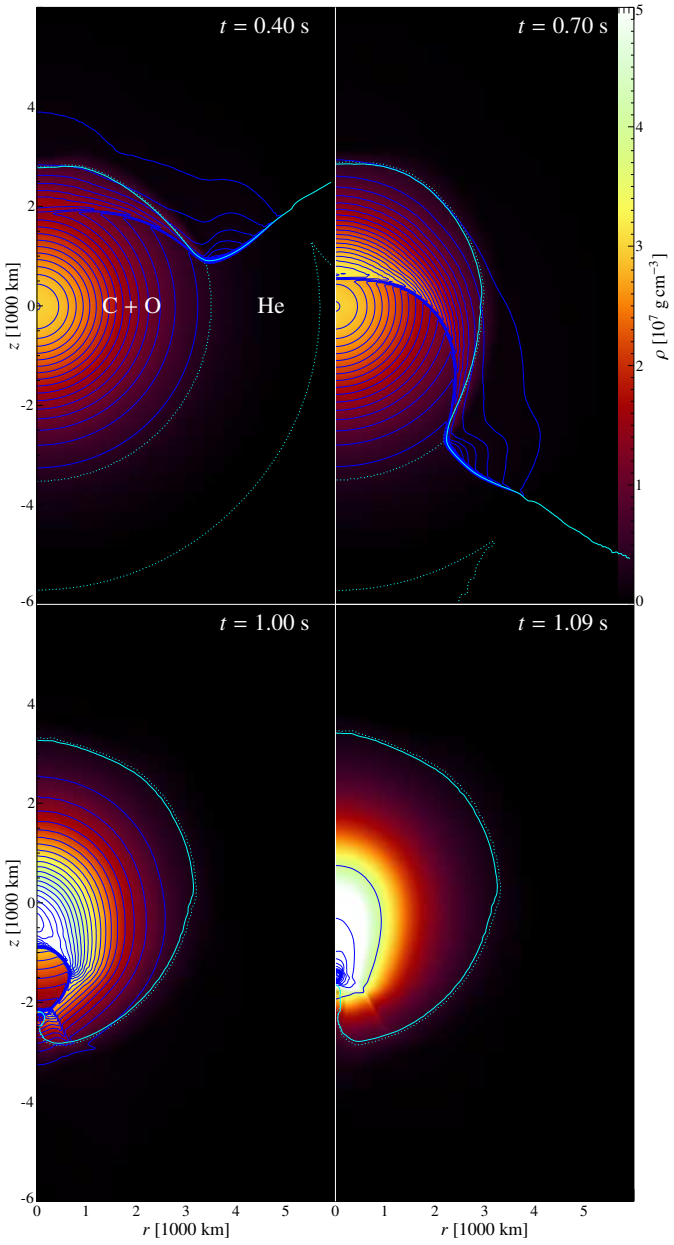

Fig. 5. Time evolution of the model z4.24A_2d_256.

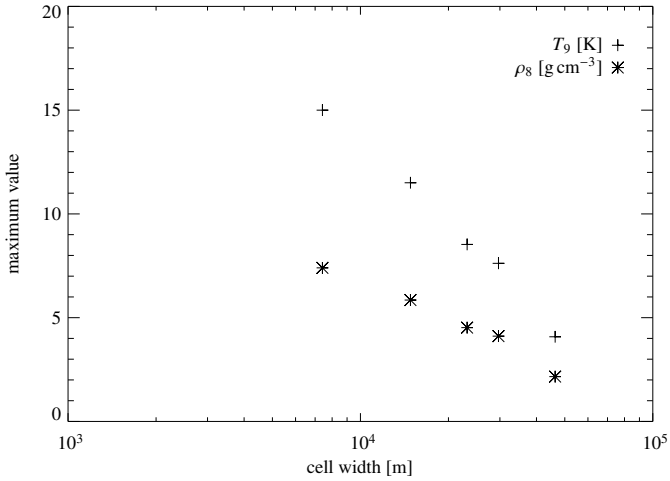

Fig. 6. Resolution study of the maxima in the central shock collision of model z4.24A_2d.

and densities became apparent – an effect that is discussed in Sect. 3.2 below.

Finally, a series of models with a different initial mass distribution was investigated. Sequence "B" corresponds to models with 0.9 $M_\odot$ of C/O and 0.1 $M_\odot$ of He and the parameters given in Table 3. They support the generality of the results discussed above. The dependence on the initial flame geometry is analogous to case "A", but maximum densities and temperatures achieved are generally lower. This is consistent with the fact that the shock waves originating from the He shell have to cross a larger pressure gradient before they reach the center in model "B".[5] Still, most of the models reach the conditions for core ignition described in Sect. 2.4 (the "z*r*" models did not ignite with mass distribution "A" either).

3.2. A resolution study

The numerical resolution of the parameter study presented above was relatively low with a spatial resolution of 23.2 km only. Hence, for one of the most interesting models, z4.24A_2d_256, we performed a resolution study. Globally, we found a good agreement of the temporal evolution of the state variables. But the maximum densities and temperatures at the central shocks collision showed a significant dependence on the numerical resolution of the simulation (see Fig. 6). With decreasing cell size the maximum values increase almost exponentially. This trend continues down to the smallest tested cell width (7.4 km) and no indication for numerical convergence is found. Given that the shock collision is an almost perfect spherically symmetric problem, we reduced to one dimension in order to facilitate even higher resolutions. The state variables on the r-axis of simulation s4.10A_2dq_256 at $t = 0.25$ s linearly interpolated to higher resolutions were taken as initial condition. The results of the corresponding one-dimensional runs with increasing resolution are presented in Fig. 7. It shows an analogous exponential increase of the temperature and density maxima down to a cell width of 0.72 km. Below that value, however, the temperatures exceeded the limits of our equation of state. Here, more micro-physical processes would have to be taken into account and could restrict further growth of density and temperature.

But even without this restriction, from analytical considerations it is clear that the density growth ratio must be limited, although it can get very big. In the idealized case of infinitely strong shock reflection at the origin in spherical geometry (and constant initial conditions of $\rho_0(r) = 1$, $u_0(r) = -1$, and $p_0(r) = 0$), its value is $\left(\frac{\gamma+1}{\gamma-1}\right)^3$ after the reflected shock (cf. Glaister 1988).[6] Another problem that can be solved semi-analytically

[5] Geometrical amplification effects do not play a role at such big radii.

[6] For an ultra-relativistic degenerate gas like in a WD's center $\gamma = \frac{4}{3}$ holds in good approximation and thus $\left(\frac{\gamma+1}{\gamma-1}\right)^3 = 7^3 = 343$.

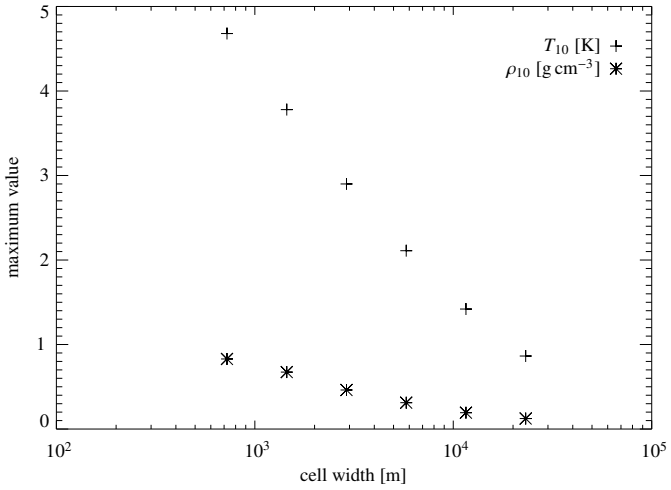

Fig. 7. One-dimensional resolution study of the maxima in the central shock collision of model s4.10A.

is that of a spherical shock wave that starts from infinity, converges to the origin, and is reflected there (cf. Guderley 1942; Landau & Lifschitz 1991; Ponchaut et al. 2006). While the shock is moving inwards it grows in strength because of its surface decrease. Close enough to the center for the strong shock approximation to hold, it can be shown that $p \sim r^{-\frac{2(1-n)}{n}}$, $\rho = \text{const}$, and $|u| \sim r^{-\frac{1-n}{n}}$ with n being a constant between 0 and 1 that has to be numerically determined and depends only on the ratio of specific heats γ. According to Landau & Lifschitz (1991), at the time of perfect focusing the density has increased by a factor of 20.1 for $\gamma = \frac{7}{5}$ and the reflection is accompanied by another increase by about a factor of 145. Thus a maximum compression of about 2,900 can be achieved and in the case of $\gamma = \frac{4}{3}$, relevant in our case, those numbers are even bigger.

In our simulations the shock that propagates inwards into the WD due to the He detonation is followed by an extended wave of matter that is also flowing inwards. Therefore the case might lie somewhere in between these two idealized situations: The shock is amplified by the geometrical focusing effect and thus compresses a significant part of the core that is then burned at higher densities. On the other hand the matter succeeding the in-flowing shock leads to even higher densities after the shock is reflected. Taking all those properties into account, it becomes clear why the ignition conditions for a core detonation can be fulfilled so well in our simulations. Provided that the shock is symmetric enough also an off-center ignition at a point with much smaller initial density like in model z4.24A_2d_256 is possible in this scenario.

As the minimum shock surface that we can reach depends on the grid resolution, the maximum temperature and density values that are achieved through the geometric amplification in the shock implosion naturally also do so. In our simulations a successful second detonation ignition thus depends on the resolution and it seems likely that all the models in Table 3 would explode provided that they were well enough resolved.

Therefore, the results given in Table 3 have to be interpreted as a conservative estimate of the possibility of a detonation ignition. If at a certain grid resolution the ignition conditions are fulfilled, a second core detonation must happen. However, if the ignition conditions are not fulfilled a core detonation can still not be excluded and might be achieved with increasing resolution[7].

Table 4. Results of three complete double detonation simulations. All nucleosynthetic abundances are given in solar masses. $M_{\rm loss}$ is the mass loss over the grid boundaries.

Model	^{12}C+^{16}O	^{56}Ni	^{28}Si	$M_{\rm loss}$
z4.24A_2d_128	0.01	0.40	0.51	0.08
z4.24A_3d_128	0.01	0.45	0.50	0.05
s4.10A_2dq_128	0.02	0.41	0.50	0.08

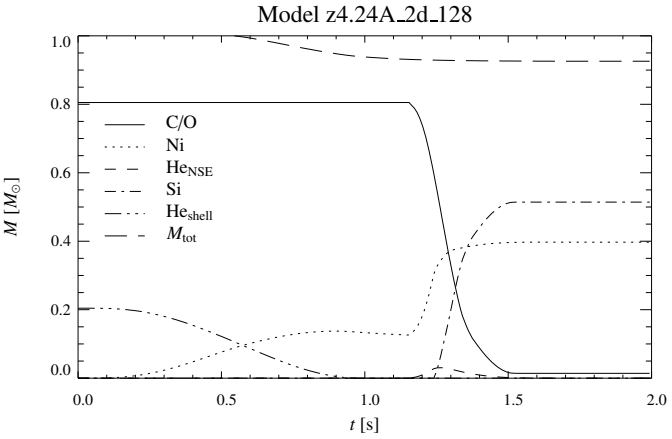

Fig. 8. Time evolution of the mass fractions of model z4.24A_2d_128.

3.3. Three double-detonation supernova simulations

As a first step to compare the simulations of sub-Chandrasekhar mass models with actual SN Ia observations, measurable quantities like the nucleosynthetic abundances of an explosion have to be determined. To this end, two complete double detonations of model z4.24A until $t = 2.0$ s have been simulated. One of them was set up in 3D with 256^3 cells for the full WD. For comparison with previous results, the second, 2D rotationally symmetric simulation was also done with this low resolution (128×256 cells).

In order to test the influence of symmetry in the initial flame configuration in the He shell on the explosion abundances, besides these maximally asymmetric cases a 2D double detonation of the spherically symmetric model s4.10A was also simulated. The results of all three simulations are given in Table 4. For model z4.24A_2d_128 also the time evolution of the mass fractions of the reduced network is plotted in Fig. 8 and will be discussed in the following.

At first, the ^{4}He in the shell is burnt completely to ^{56}Ni. But the mass of the latter is somewhat reduced due to some mass loss through the boundaries of the computational domain. This is clearly visible also in the decrease of the total mass. The reason for this is that the co-expanding grid was set up to track a mass shell at 0.85 $M_\odot$. Since the matter above this shell expands with a larger velocity, some of it leaves the numerical grid. The

[7] Note that in this case the minimum detonator volume may be the limiting constraint.

tracking of a bigger mass shell would reduce this mass loss, but it would also reduce the resolution of the colliding shocks in the core.

After about 1.2 s the collision of the shock waves resulting from the He detonation gives rise to conditions for a detonation in the C + O core. In the corresponding grid zones, this detonation was artificially triggered by setting up a second level set. At the high densities near the center the C/O mixture is burnt completely to ^{56}Ni in NSE with a small amount of ^{4}He. But the ^{4}He recombines to ^{56}Ni after a short time due to the density decrease caused by expansion. Farther away from the center at smaller densities the burning product is ^{28}Si and some low-density matter at the border of the core remains unburnt. In this way 0.40 $M_\odot$ of ^{56}Ni and 0.51 $M_\odot$ of ^{28}Si are produced after about 1.5 s and 0.01 $M_\odot$ of C/O remain unburnt.

The results of the 3D case z4.24A_3d_128 are very similar to the 2D one. However, 0.05 $M_\odot$ more ^{56}Ni were produced. The main reason for this difference is the loss of different amounts of mass over the boundaries of the computational domain, which amounted to 0.08 $M_\odot$ in 2D and only 0.05 $M_\odot$ in 3D. The explanation for the smaller mass loss is a simple geometric effect: In 3D cartesian coordinates there is more volume outside the star that lies on the numerical grid than in 2D cylinder coordinates. For example, the largest distance from the center is the length of the space diagonal ($\sqrt{3}\,a$, when a is the side length), whereas in 2D it is the length of the diagonal in the rz-plane ($\sqrt{2}\,a$).

Due to the spherical symmetry in the model s4.10A_2dq_128 He burning and shock convergence are faster. Therefore all the reactions finish already after about one second, but according to Table 4, almost the same nucleosynthetic abundances are produced. This indicates that the density distribution in the core in case of shocks converging asymmetric to the density distribution differs only slightly from the perfect spherical symmetric case. As the now following core detonation propagates supersonic, the final abundances are independent of the position of the ignition point.

In all three cases considered the ^{56}Ni-mass and with it the explosion energy are rather large. In fact, they reach the range of (weaker) *normal* SNe Ia. However, these numbers have to be taken with care since the density limit of $3 \cdot 10^7$ g cm^{-3} adopted here for separating burning of C/O to ^{56}Ni and ^{28}Si, respectively, is quite uncertain, but will have an impact on the final abundances.

4. Summary and conclusions

We have studied the sub-Chandrasekhar model of SNe Ia by means of a series of two-dimensional and a few three-dimensional simulations with different initial conditions. The numerical scheme used is based on the PPM algorithm, and the propagation of the detonation front is modeled applying the level set technique. This novel implementation allowed for an accurate treatment of the hydrodynamic features of the sub-Chandrasekhar model (such as shock waves and thin detonation fronts) in multiple dimensions.

With our generic 1-$M_\odot$ model we performed a parameter study involving different He masses and ignition geometries of the initial He detonation. We find that a detonation in the He shell can clearly trigger a second detonation in the core and at least for the mass configurations studied, the double detonation seems to be a very robust process, which works without any "fine-tuning" of our model parameters. In almost all of the simulations performed, the ignition conditions for a core detonation were reached at or near the center of the WD as a result of the convergence of the shock from the He shell detonation and in the few other cases the failure is likely a result of the finite numerical resolution. The high maximum densities and temperatures that are needed for detonation ignition and the fact that the shock is not diluted too much when propagating inwards against the pressure gradient are made possible through a geometrical shock amplification effect that appears in spherical symmetry: As the surface of the shock decreases its strength has to increase. The high compression that can be achieved theoretically in this way, especially if full convergence is reached and the shock is reflected (cf. Sect. 3.2), could even allow successful double detonations with considerably smaller He masses. The shock amplification that is reached, however, turns out to be resolution dependent on the numerical grid as it is coupled to the smallest resolvable shock surface. Taking this into account it is very likely that all our models would explode, if they were simulated with sufficiently high resolution.

The question of whether an incineration could also happen directly at the core–shell interface, was not addressed here. This could of course prevent the spherical shock convergence mechanism from playing a role, at least in parts of the parameter space. Therefore, edge-lit detonations are postponed to a separate study.

The complete double detonation simulations that were performed for the models z4.24A and s4.10A resulted in ^{56}Ni-masses of about 0.40 to 0.45 $M_\odot$. Are the studied events thus good candidates for normal SNe Ia? Most likely not. Starting with a He-shell detonation, all of our models show a significant amount of rapidly expanding ^{56}Ni in the outer layers. In the observed spectra of normal and sub-luminous events, however, this was never found up to now (cf. Hillebrandt & Niemeyer 2000). The only exception is the super-luminous SN 1991T. Thus our solar-mass models most likely will not be able to explain normal or sub-luminous SNe Ia and, given the robustness of the explosion mechanism of the model, the only conceivable explanation for the lack of observations of corresponding SN Ia events is that the progenitors are not realized in nature – or are very rare.

For a better agreement with observations a reduction of the He-shell mass would be the most obvious choice. However, then a significantly larger core mass would most likely be required, because otherwise the He would not detonate. In this case the core density would be much higher resulting in a very large Ni mass. This would again not be a candidate for normal SNe Ia, but it might be a promising candidate for objects like SN 1991T.

Further work could cover model improvements like a more realistic nuclear network including the calculation of real reaction rates depending on the actual thermodynamic state of the burnt matter. This would make an investigation of the onset and

the explosion dynamics of the core detonation possible. Also, more extended parameter studies, especially towards the lower end of possible He masses, would be interesting. For a comparison with observations the calculation of synthetic light curves and spectra would also be desirable.

Acknowledgements. We want to thank Konstantinos Kifonidis who helped with the implementation of the Marquina solver and Ewald Müller for many helpful discussions. The simulations presented here were carried out at the Computer Center of the Max Planck Society, Garching, Germany. This work was supported by the Deutsche Forschungsgemeinschaft via the Transregional Collaborative Research Center TRR 33 "The Dark Universe".

References

Arnett, D. 1997, in NATO ASIC Proc. 486: Thermonuclear Supernovae, ed. P. Ruiz-Lapuente, R. Canal, & J. Isern, 405
Benz, W. 1997, in NATO ASIC Proc. 486: Thermonuclear Supernovae, ed. P. Ruiz-Lapuente, R. Canal, & J. Isern, 457
Blinnikov, S. I. & Khokhlov, A. M. 1986, Soviet Astronomy Letters, 12, 131
Branch, D., Livio, M., Yungelson, L. R., Boffi, F. R., & Baron, E. 1995, PASP, 107, 1019
Colella, P. & Glaz, H. M. 1985, Journal of Computational Physics, 59, 264
Colella, P. & Woodward, P. R. 1984, Journal of Computational Physics, 54, 174
Courant, R. & Friedrichs, K. O. 1948, Supersonic flow and shock waves (Pure and Applied Mathematics, New York: Interscience, 1948)
Donat, R. & Marquina, A. 1996, Journal of Computational Physics, 125, 42
Fryxell, B. A., Müller, E., & Arnett, W. D. 1989, MPA Preprint, 449
Gamezo, V. N., Khokhlov, A. M., & Oran, E. S. 2004, Physical Review Letters, 92, 211102
Gamezo, V. N., Khokhlov, A. M., Oran, E. S., Chtchelkanova, A. Y., & Rosenberg, R. O. 2003, Science, 299, 77
García-Senz, D., Bravo, E., & Woosley, S. E. 1999, A&A, 349, 177
Glaister, P. 1988, International Journal for Numerical Methods in Fluids, 8, 97
Golombek, I. & Niemeyer, J. C. 2005, A&A, 438, 611
Guderley, G. 1942, Luftfahrtforschung, 19, 302
Han, Z. & Podsiadlowski, P. 2004, MNRAS, 350, 1301
Hillebrandt, W. & Niemeyer, J. C. 2000, ARA&A, 38, 191
Imshennik, V. S. & Khokhlov, A. M. 1984, Soviet Astronomy Letters, 10, 262
Khokhlov, A. M. 1991, A&A, 246, 383
Landau, L. D. & Lifschitz, E. M. 1991, Hydrodynamik (Lehrbuch der theoretischen Physik, Akademie-Verlag, 1991)
Livio, M. 2000, in Type Ia Supernovae, Theory and Cosmology. Edited by J. C. Niemeyer and J. W. Truran. Published by Cambridge University Press, 2000., p.33, ed. J. C. Niemeyer & J. W. Truran, 33
Livne, E. 1990, ApJ, 354, L53
Livne, E. 1997, in NATO ASIC Proc. 486: Thermonuclear Supernovae, ed. P. Ruiz-Lapuente, R. Canal, & J. Isern, 425
Livne, E. & Glasner, A. S. 1990, ApJ, 361, 244
Livne, E. & Glasner, A. S. 1991, ApJ, 370, 272
Mazzali, P. A., Röpke, F. K., Benetti, S., & Hillebrandt, W. 2007, Science, 315, 825
Mulder, W., Osher, S., & Sethian, J. A. 1992, Journal of Computational Physics, 100, 209
Napiwotzki, R., Karl, C. A., Nelemans, G., et al. 2005, in Astronomical Society of the Pacific Conference Series, Vol. 334, 14th European Workshop on White Dwarfs, ed. D. Koester & S. Moehler, 375
Niemeyer, J. C. & Woosley, S. E. 1997, ApJ, 475, 740
Nomoto, K., Uenishi, T., Kobayashi, C., et al. 2003, in From Twilight to Highlight: The Physics of Supernovae, ed. W. Hillebrandt & B. Leibundgut, 115
Osher, S. & Sethian, J. A. 1988, Journal of Computational Physics, 79, 12
Parthasarathy, M., Branch, D., Jeffery, D. J., & Baron, E. 2007, New Astronomy Review, 51, 524
Plewa, T., Calder, A. C., & Lamb, D. Q. 2004, ApJ, 612, L37
Ponchaut, N. F., Hornung, H. G., Pullin, D. I., & Mouton, C. A. 2006, Journal of Fluid Mechanics, 560, 103
Reinecke, M., Hillebrandt, W., & Niemeyer, J. C. 1999a, A&A, 347, 739
Reinecke, M., Hillebrandt, W., & Niemeyer, J. C. 2002a, A&A, 386, 936
Reinecke, M., Hillebrandt, W., & Niemeyer, J. C. 2002b, A&A, 391, 1167
Reinecke, M., Hillebrandt, W., Niemeyer, J. C., Klein, R., & Gröbl, A. 1999b, A&A, 347, 724
Reinecke, M. A. 2001, PhD thesis, Technical University of Munich
Röpke, F. K. & Hillebrandt, W. 2005, A&A, 431, 635
Röpke, F. K., Hillebrandt, W., & Niemeyer, J. C. 2004a, A&A, 420, 411
Röpke, F. K., Hillebrandt, W., & Niemeyer, J. C. 2004b, A&A, 421, 783
Röpke, F. K., Hillebrandt, W., Niemeyer, J. C., & Woosley, S. E. 2006, A&A, 448, 1
Röpke, F. K., Hillebrandt, W., Schmidt, W., et al. 2007a, ArXiv Astrophysics e-prints, 707
Röpke, F. K. & Niemeyer, J. C. 2007, A&A, 464, 683
Röpke, F. K., Niemeyer, J. C., & Hillebrandt, W. 2003, ApJ, 588, 952
Röpke, F. K., Woosley, S. E., & Hillebrandt, W. 2007b, ApJ, 660, 1344
Ruiz-Lapuente, P., Blinnikov, S., Canal, R., et al. 2000, Memorie della Societa Astronomica Italiana, 71, 435
Schmidt, W. & Niemeyer, J. C. 2006, A&A, 446, 627
Schmidt, W., Niemeyer, J. C., Hillebrandt, W., & Röpke, F. K. 2006, A&A, 450, 283
Sharpe, G. J. 1999, MNRAS, 310, 1039
Smiljanovski, V., Moser, V., & Klein, R. 1997, Combustion Theory Modelling, 1, 183
Stritzinger, M., Leibundgut, B., Walch, S., & Contardo, G. 2006, A&A, 450, 241
Wiggins, D. J. R. & Falle, S. A. E. G. 1997, MNRAS, 287, 575

Wiggins, D. J. R., Sharpe, G. J., & Falle, S. A. E. G. 1998, MNRAS, 301, 405
Woosley, S. E. 1990, Type I Supernovae: Carbon Deflagration and Detonation, ed. A. G. Petschek (New York: Springer-Verlag), 182
Woosley, S. E., Taam, R. E., & Weaver, T. A. 1986, ApJ, 301, 601
Woosley, S. E. & Weaver, T. A. 1994, ApJ, 423, 371

List of Objects